minerals

MDPI

Article

Magmatic Garnet and Magma Evolution in Cuonadong Leucogranites: Constraints from Petrology and Mineral Geochemistry

Haibo Yan [1,2], Deshui Yu [3,*], Shoujing Wang [3] and Chi Ma [3]

[1] State Key Laboratory of Isotope Geochemistry, Guangzhou Institute of Geochemistry, Chinese Academy of Sciences, Guangzhou 510640, China
[2] CAS Center for Excellence in Deep Earth Science, Guangzhou 510640, China
[3] Zhengzhou Institute of Multipurpose Utilization of Mineral Resources, Chinese Academy of Geological Sciences, Zhengzhou 450006, China
* Correspondence: yudeshui_jlu@163.com

Abstract: Located at the eastern segment of the Tethyan Himalayan tectonic unit, the Cuonadong leucogranites (muscovite granite and pegmatite) have a mineral assemblage of quartz, plagioclase, and alkali feldspar, as well as muscovite and garnet. Garnets in both muscovite granite and pegmatite belong to the almandine–spessartine solid solution, with minor andradite, grossular, and pyrope, and show a specific Mn zoning of a relatively rim-ward Mn depletion trend. However, a few garnets in pegmatite show grossular enrichment towards the rim. All the analyzed garnets are characterized by HREE enrichment and LREE depletion with obvious Eu anomalies. The difference is that garnets from the muscovite granite show distinct left-declined or flat HREE patterns, while those from the pegmatite are featured by flat or right-declined HREE patterns. Moreover, garnets from the pegmatite show relatively more distinct HREE- and Y-rich cores compared with those from the muscovite granite. The MnO concentration, spessartine content, and MnO/(MnO + FeO) ratio of the garnets from the Cuonadong dome increase from the muscovite granite to the pegmatite, suggesting that the pegmatite likely formed from a more evolved environment. Elevated grossular and CaO contents of the garnet rim in the pegmatite may reflect an influence of fluids in their composition. The major and trace element compositions and zoning textures of garnets from the Cuonadong leucogranites suggest a magmatic origin and a formation at moderately low temperatures and relatively low-pressure conditions. From the muscovite granite to the pegmatite, the system entered a fluid-rich environment and the garnets from the pegmatite likely crystallized from a lower-temperature fluid.

Keywords: leucogranite; garnet; geochemistry; magma evolution; Tethyan Himalaya

check for updates

Citation: Yan, H.; Yu, D.; Wang, S.; Ma, C. Magmatic Garnet and Magma Evolution in Cuonadong Leucogranites: Constraints from Petrology and Mineral Geochemistry. *Minerals* **2022**, *12*, 1275. https://doi.org/10.3390/min12101275

Academic Editor: Nikita V. Chukanov

Received: 20 August 2022
Accepted: 7 October 2022
Published: 9 October 2022

1. Introduction

The Himalayan orogenic belt is the product of the Cenozoic India–Eurasia collision. In the middle and late period of the collision (Late Eocene–Miocene), the crustal material underwent intense anatexis [1,2], and formed two granite belts extending thousands of kilometers, namely, the Tethyan Himalayan leucogranite belt and the High Himalayan leucogranite belt [3]. The Tethyan Himalayan leucogranite belt, located in the northern part of the Himalayan orogenic belt, has potential rare metal resources related to granite, such as Li, Be, Nb, Ta, W, and Sn [3–10]. The Cuonadong dome, located in the eastern segment of the Tethyan Himalayan tectonic unit, is the first dome in the Himalayan orogenic belt to be explored and delineated for rare polymetallic ore bodies [11]. The leucogranite of Cuonadong is distributed in the core of the dome.

Granitic melts not only experience solidification and crystallization but also magmatic–hydrothermal processes, even at the late stage of magmatic evolution [12,13]. The magmatic–hydrothermal process at the late stage of magmatic evolution has been recorded especially

in highly fractionated granite [12,14]. Minerals usually record the evolution history of granitic magmas [15–18], such as garnet, apatite, and tourmaline. Garnet, as a common accessory mineral in leucogranite, is widely distributed in the Cuonadong dome, and its texture and chemical changes record important information about the process of granitic magma evolution [19,20]. On the one hand, the different components of garnet can reflect the formation environment and genesis of granitic magma. On the other hand, garnet is usually enriched with trace elements such as REE, Zr, Hf, and Y, and the geochemical behavior of these elements can indicate the evolution of granitic magma [21–24]. Volatile and magmatic fluid phases are separated from the melt at the late stage during the crystallization of highly fractionated granite [16,18,25,26]. Thus, garnet is widely used to indicate the degree of granitic magma evolution and forming conditions [27–30].

A great deal of research has been done on Cuonadong leucogranite, mainly focusing on geochronology, geochemistry, mineralogy, and petrogenesis [7–9,11,31–34]. However, there are still few studies on the elemental evolution characteristics of minerals between different types of leucogranite, the physicochemical conditions for the mineral formation, and the magmatic evolution process.

In this paper, the garnets in the muscovite granite and pegmatite from the Cuonadong dome were selected as the research object, and the major and trace element geochemical characteristics of garnet were analyzed by electron microprobe analysis (EPMA) and laser ablation inductively coupled plasma mass spectrometry (LA–ICP–MS). The main aims are to (1) find out the origin of garnet in the Cuonadong leucogranite; and (2) reveal the magma evolution process of the Cuonadong leucogranites through the geochemical characteristics of garnet.

2. Geological Setting

From north to south, the Himalayan terrane is mainly composed of four tectonic units: Tethyan Himalayan Sequence (THS), High Himalayan Crystalline Sequence (HHCS), Lesser Himalayan Sequence (LHS), and Sub-Himalayan Sequence (SHS) (Figure 1), and their structural boundaries are the Indus-Yarlung Zangbo Suture Zone (IYZSZ), South Tibetan Detachment System (STDS), Main Central Thrust (MCT), Main Boundary Thrust (MBT), and Main Front Thrust (MFT) [35–37].

Located between the IYZSZ and the STDS (Figure 1), the THS is mainly a set of sedimentary rocks, including sandstone, siltstone, mud shale, and low-grade metamorphic slate and phyllite [38–41]. The HHCS lies between the STDS and the MCT and is composed of a series of high-grade metamorphic sedimentary rocks [32,42].

The Himalayan leucogranites are mainly distributed in the E–W direction (Figure 1). The northern belt is the Tethyan Himalayan leucogranite belt. The Tethyan Himalayan leucogranites are mostly produced in the core of the Tethys Himalayan gneiss dome [43] or intruded into the THS, with representative leucogranites from east to west, including Yalhashangbo, Cuonadong, Rampa, Kangmar, Lhagai Kangri, Malashan, and others [3,44,45]. The southern belt is the High Himalayan leucogranite belt, which is distributed around the STDS and intruded the HHCS as sheets with various scales, and is represented by Khula Kangri, Dinggye, Jilong, and other leucogranites from east to west [46,47].

A large number of Au–Sb, Pb–Zn–Sb, and Pb–Zn polymetallic deposits are produced in the THS, forming an Au–Sb–Pb–Zn Tethyan Himalayan metallogenic belt with a 600 km E–W extension, which is an important Pb–Zn–Au–Sb resource base on the Qinghai-Tibet Plateau [48,49]. These Au–Sb–Pb–Zn deposits are mainly distributed along the Himalayan dome, showing the spatial distribution characteristics of zoning, sheeting, and clustering, and showing the characteristics of an annular mineralization zoning centered on the dome [50,51]. Be–Rb–Nb–Ta–W–Sn and other rare metal deposits discovered in Cuonadong, Lalong, Cuore, and other places reveal the metallogenic potential of Himalayan rare metals, which are also mainly developed in the dome [4–6].

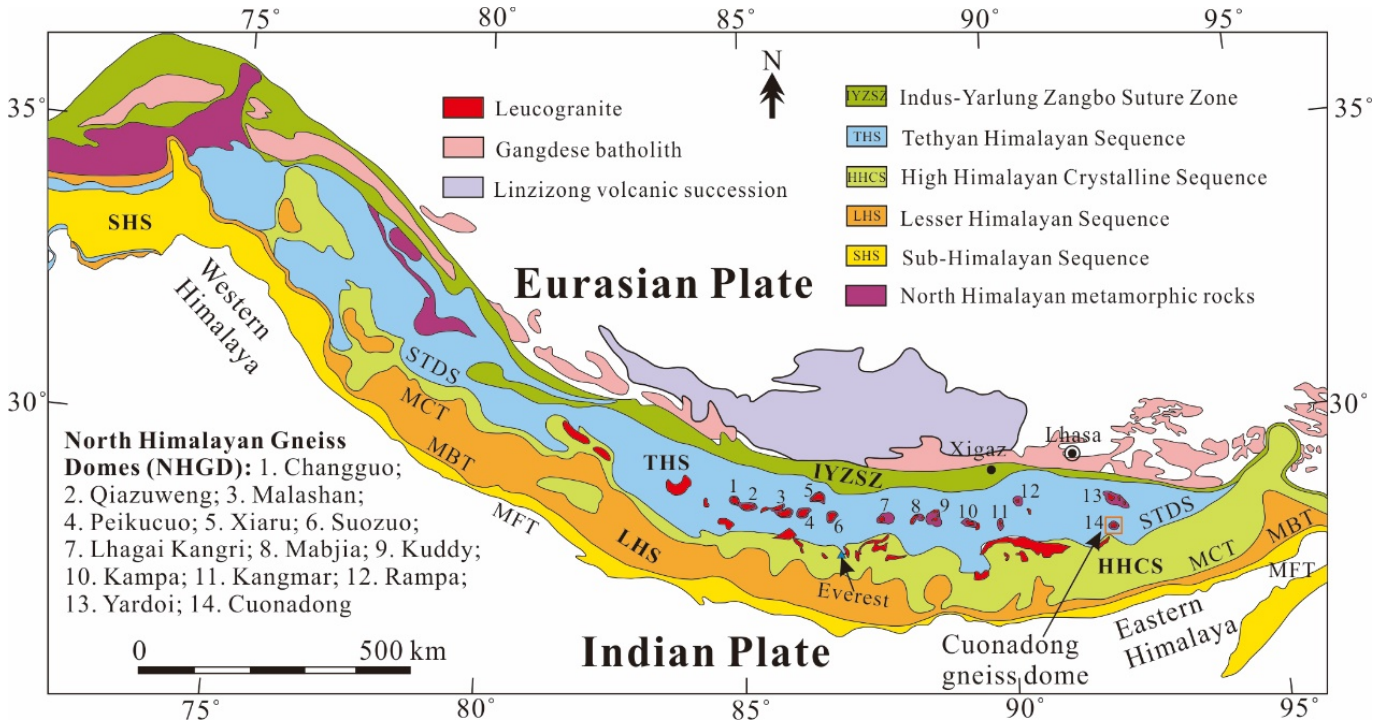

Figure 1. Simplified geological map showing the distribution of the Himalayan leucogranite, gneiss dome, and tectonic zones (modified after [3,10,52]).

3. Geology of the Cuonadong Dome

The Cuonadong gneiss dome with an area of ca. 100 km^2 is located in the eastern segment of the Tethyan Himalayan tectonic unit, adjacent to the South Tibetan Detachment System (STDS) (Figure 1). The Cuonadong gneiss dome can be divided into three parts from outside to inside: cap layer (rim), detachment system (mantle), and core (Figure 2, [4,39,53]). The cap layer is mainly Jurassic Ridang Formation and Triassic Nieru Formation low-grade metamorphic rocks, and the lithology is mainly argillaceous silty slate, schist, and phyllite [54,55]. Between the upper overburden and the dome core is the detachment system, which is bounded by the upper detachment fault and the lower detachment fault, respectively [56]. The detachment system is mainly composed of a garnet–kyanite–staurolite–biotite schist with medium-thin layers of skarnized marble, followed by a sillimanite-bearing granitic gneiss, tourmaline-bearing granitic gneiss, and garnet-bearing muscovite gneiss, and the degree of metamorphism gradually deepens from top to bottom [33,54]. Furthermore, a large number of pegmatite dikes are developed in a core and a mantle [4,54]. The core mainly consists of a Neoproterozoic–Early Paleozoic granitic gneiss and Cenozoic leucogranites (mainly two-mica granite, muscovite granite, tourmaline granite, garnet granite, and pegmatite) [33,57,58]. Previous studies suggest that the Cuonadong leucogranites are highly evolved granites that have undergone high degree of crystallization and fractionation during the ascending emplacement of magma [3,7,8,11].

Since the Cenozoic, the magmatism developed in the Cuonadong dome includes (1) Oligocene (ca. 34–26 Ma) deformed two–mica granite and pegmatite [53,59]; (2) Early Miocene (ca. 24–17 Ma) weakly deformed two-mica granite [8,57,60]; and (3) Middle Late Miocene (ca. 16–14 Ma) undeformed garnet-, tourmaline-, and muscovite-bearing granite and beryl-bearing pegmatite [7,9,61]. However, the ages of the Cuonadong leucogranites published in large numbers are around 22–14 Ma.

In recent years, a large number of deposits have been discovered in the Cuonadong dome, including skarn-type and/or hydrothermal vein-type Be–W–Sn deposits and granite–pegmatite-type Be–W–Sn–Rb deposits [4–6,8–10,56].

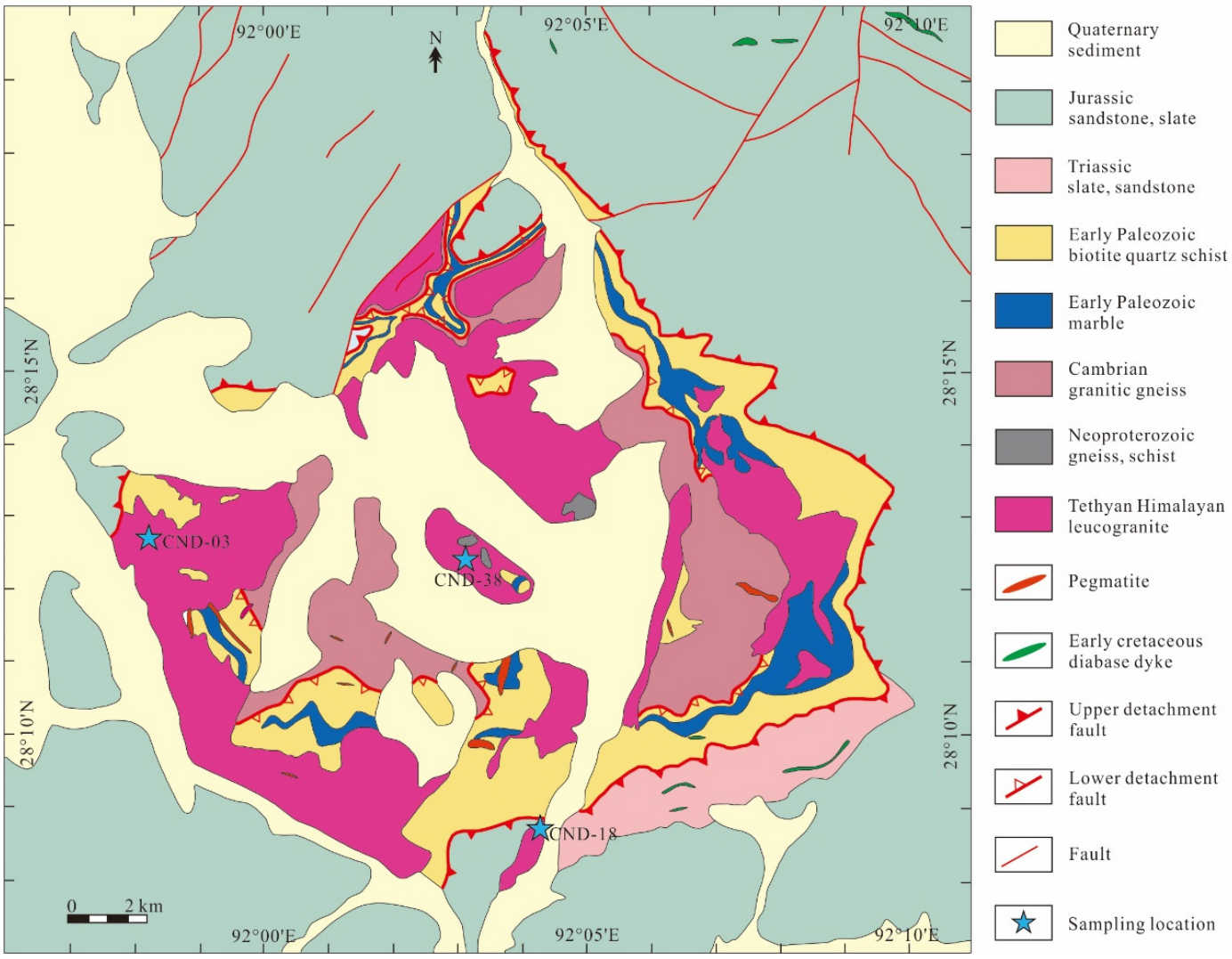

Figure 2. Geological map of the Cuonadong gneiss dome (modified after [8,58]).

4. Samples and Analytical Methods

4.1. Sample Description

A total of three samples were used for the chemical analysis of garnet in this paper. The muscovite granite (CND–03) was collected from the western part of the Cuonadong dome, and the pegmatite samples, CND–18 and CND–38, were collected from the southern and central parts of the Cuonadong dome, respectively. The sampling locations are shown in Figure 2. Muscovite granite is gray-white, with a medium- and fine-grained granite texture and massive structure. Major mineral compositions include quartz (~35–40 wt%), alkali feldspar (~15–20 wt%), plagioclase (~30–35 wt%), muscovite (~7–10 wt%), garnet (~2–3 wt%), and biotite (~1–2 wt%). Garnet grains are brownish and euhedral-subhedral in hand specimens and are commonly cracked with inclusions of quartz and feldspar (Figure 3a–c). Pegmatite is white or yellowish-white, with a pegmatitic texture and massive structure, mainly composed of quartz (~35–42 wt%), alkali feldspar (~10–15 wt%), plagioclase (~35–40 wt%), muscovite (~3–5 wt%), garnet (~3–8 wt%), and biotite (~0.5–1 wt%). Garnets in the pegmatite have a reddish-brown color and show euhedral–anhedral crystals. In the investigated garnets, we found only a few inclusions (Figure 3d–i).

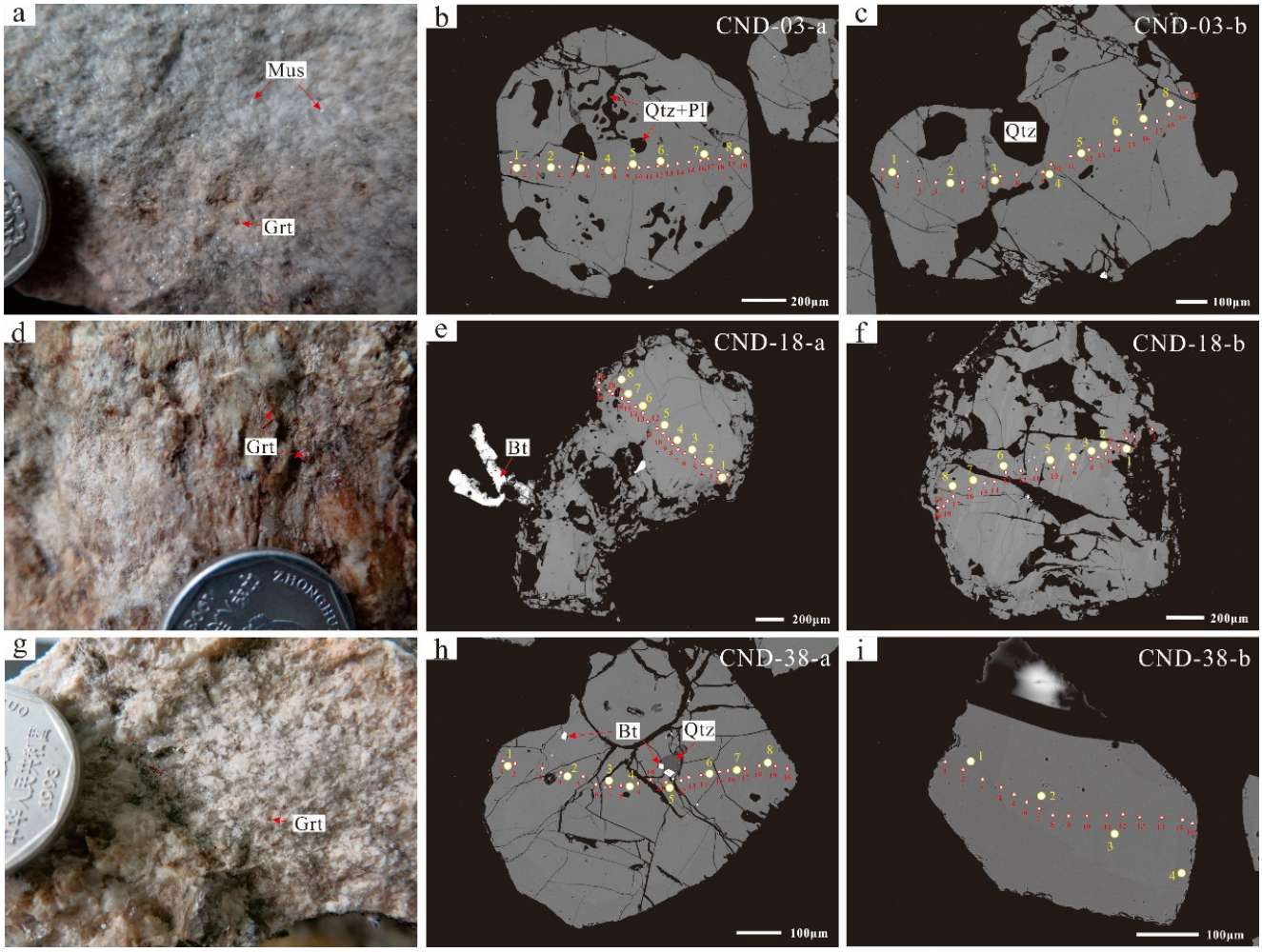

Figure 3. Representative hand specimens and back-scattered electron (BSE) images of the Cuonadong muscovite granite and pegmatite: (**a**) garnet-bearing muscovite granite; (**b**,**c**) BSE images of garnets in the muscovite granite, showing quartz and plagioclase inclusions; (**d**) garnet-bearing pegmatite; (**e**,**f**) BSE images of garnets in the pegmatite; (**g**) garnet-bearing pegmatite; (**h**,**i**) BSE images of garnets in the pegmatite showing few inclusions. Note: The red circles represent the EPMA positions, and the yellow circles represent the LA–ICP–MS analysis positions. Abbreviations: Grt = garnet; Mus = muscovite; Qtz = quartz; Pl = plagioclase; Bt = biotite.

4.2. Electron Microprobe Major Element Analysis

All the samples were placed in a vacuum chamber and coated with carbon before electron microprobe analysis (EPMA). Major elements and back-scattered electron (BSE) images of the garnet were carried out by a JEOL JXA-8230 electron microprobe at the Testing Center, Shandong Bureau of China Metallurgical Geology Bureau. The voltage was 15 kV, the current 10 nA, and the beam diameter 10 μm during the analysis. The chemical formula of garnet was calculated based on 12 oxygens.

4.3. LA–ICP–MS Trace Element Analysis

The trace elements analysis of garnet was conducted on polished thin sections using a laser ablation inductively coupled plasma mass spectrometry (LA–ICP–MS) equipped with an Agilent 7900 ICP–MS and a Resonetics RESOlution 193 nm laser at the Key Laboratory of Mineralogy and Metallogeny, Guangzhou Institute of Geochemistry, Chinese Academy of Sciences. The laser energy was 80 mJ, with a frequency of 8 Hz and a spot diameter of 60 μm. BHVO–2G, BIR–1G, BCR–2G, and SRM 610 were selected as external standard

samples in this study, while GOR132-G was used as a monitoring standard sample. Data processing was performed by ICPMS DataCal [62].

5. Results

5.1. Major Element Compositions

Major element compositions are presented in Table S1.

The garnets of the muscovite granite (CND-03) contain relatively similar contents of SiO_2 (34.8–36.4 wt%), Al_2O_3 (19.4–20.6 wt%), FeO (26.8–33.1 wt%), MnO (10.7–16.1 wt%), MgO (0.062–0.173 wt%), and CaO (0.862–1.14 wt%). Furthermore, there is little difference in the content of major elements between different garnets. Garnets of the muscovite granite predominantly belong to the almandine–spessartine with a chemical formula of $Alm_{58.13–71.81}Sps_{24.81–38.01}Adr_{1.82–3.24}Prp_{0.26–0.72}Grs_{0.00–1.41}$ (Figure 4a,b), which accounts for about 95% of the total molecular composition.

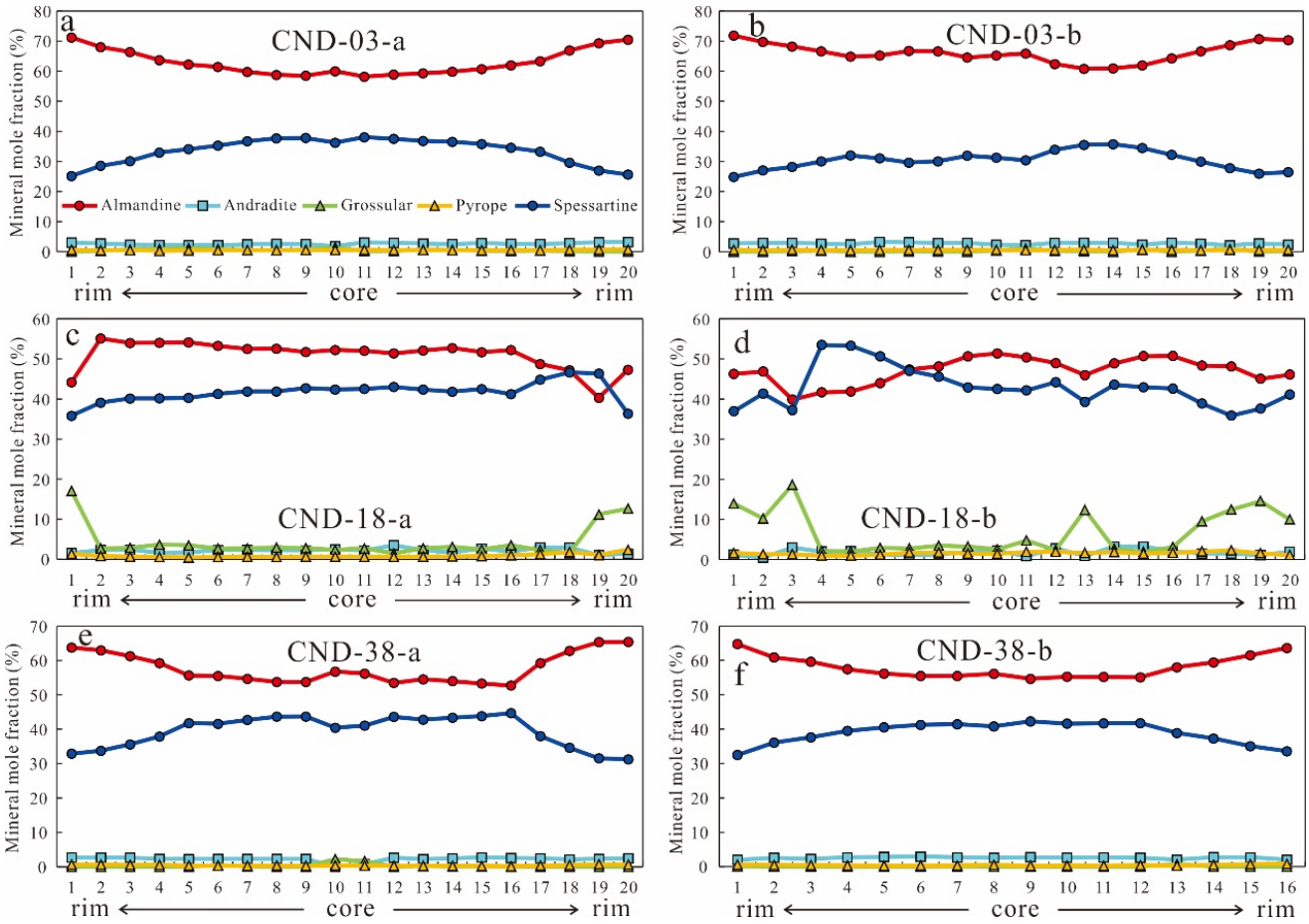

Figure 4. The core–rim chemical profiles of garnets: (**a**,**b**) garnets from the muscovite granite; (**c**–**f**) garnet grains from the pegmatite.

Compared with garnets from the muscovite granite, garnets from the pegmatite (CND-18 and CND-38) have a higher components of MnO (13.2–22.7 wt%) and spessartine (31.2–53.4 mol%) but lower FeO (18.0–30.0 wt%) and almandine (39.8–65.4 mol%) components, while the SiO_2 (35.5–36.6 wt%), Al_2O_3 (19.6–20.7 wt%), and MgO (0.030–0.583 wt%) contents are roughly similar. Similarly, garnets from the pegmatite also belong to the almandine–spessartine solid solution with a formula of $Alm_{39.81–65.39}Sps_{31.23–53.43}Adr_{0.00–3.50}Prp_{0.12–2.39}Grs_{0.00–18.60}$ (Figure 4c–f). However, it is worth noting that the CaO (1.32–7.21 wt%) and grossular (1.48–18.6 mol%) components of garnets in CND-18 are higher than those in CND-38 and CND-03.

5.2. Trace and Rare Earth Element Concentrations

The analytical results of the trace and rare earth elements are summarized in Table S2.

All the analyzed garnets are depleted in large ion lithophile elements with negative Nb and Ti and positive Ta anomalies (Figure 5). Garnets in both muscovite granite and pegmatite display low contents of Be (≤0.958 ppm), Nb (≤20.8 ppm, most <5 ppm), Ta (≤5.562), Hf (vast majority < 2), U (vast majority < 5), and Pb (vast majority < 5) and higher abundances of Y (391–3050 ppm), Ti (36.5–820 ppm), Li (67.1–286 ppm), Sn (2.06–164 ppm), and Zn (88.3–311 ppm) (Figures 6 and 7).

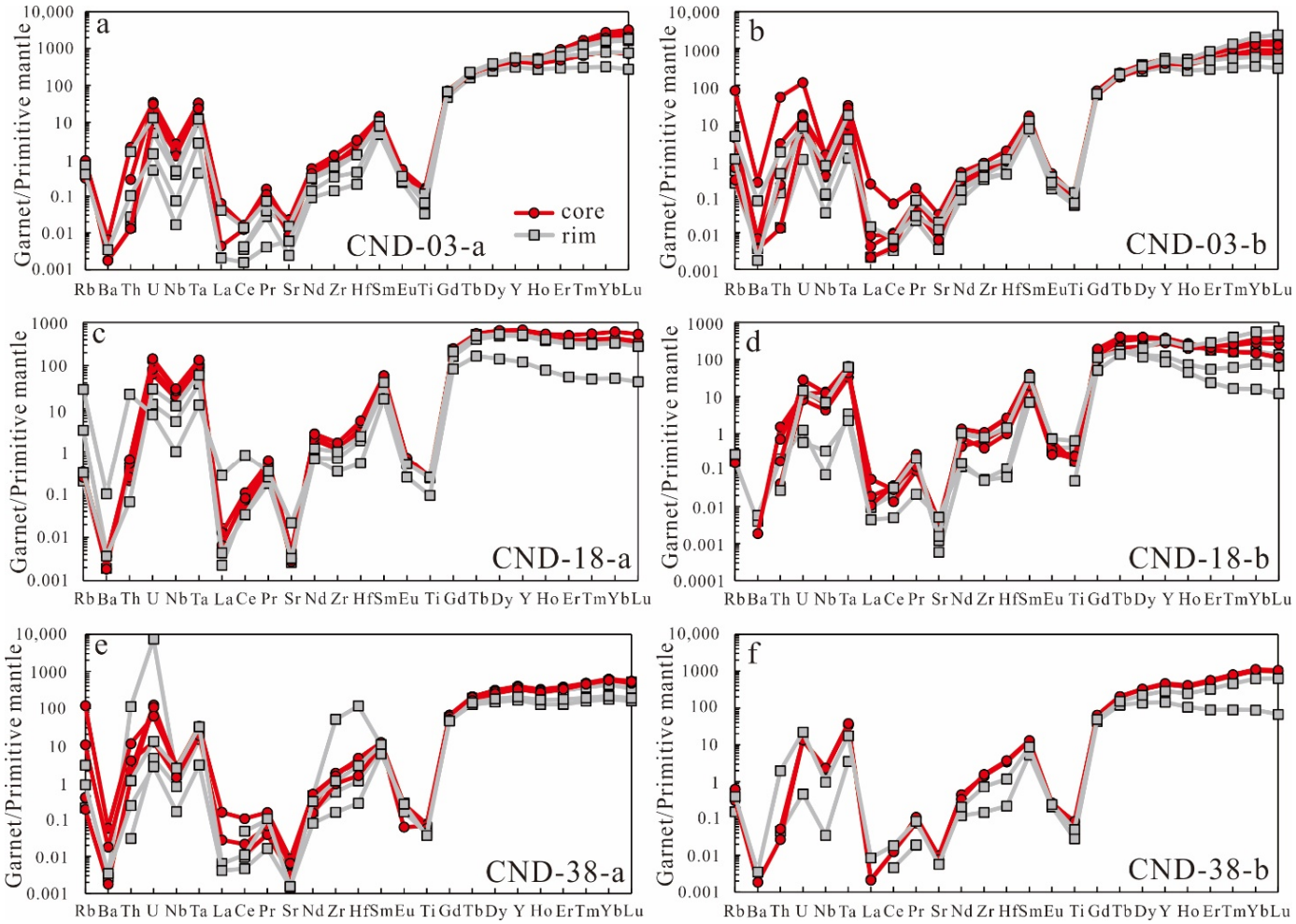

Figure 5. Primitive mantle-normalized trace element spider diagrams of garnets. (**a**,**b**) garnets from the muscovite granite; (**c**–**f**) garnet grains from the pegmatite (primitive mantle normalization data from [63]).

Rare earth element data demonstrate that garnets from the muscovite granite and pegmatite are rich in HREE (70.7–2258 ppm) and Y (391–3050 ppm) but are depleted in LREE (0.114–3.92 ppm). On the chondrite-normalized REE patterns diagrams (Figure 8), all the analyzed garnets are characterized by HREE enrichment and LREE depletion with pronounced Eu anomalies. The difference is that garnets from the muscovite granite show distinct left-declined or flat HREE patterns with HREE/LREE of 988–7926 and $(Yb/Dy)_N$ of 1.31–7.51, while garnets from the pegmatite are featured by flat or right-declined HREE patterns with HREE/LREE of 26.5–2310 and $(Yb/Dy)_N$ of 0.134–3.40.

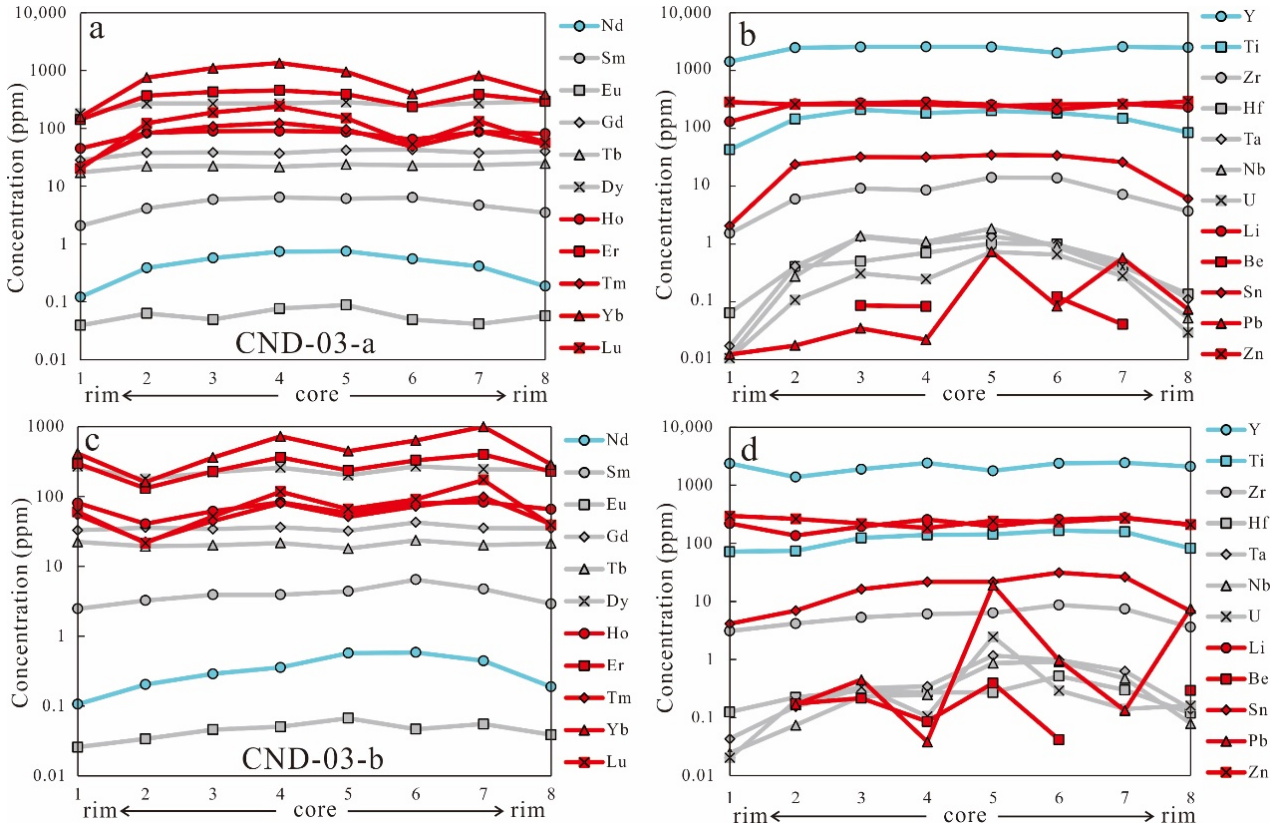

Figure 6. (**a**–**d**) Rare earth element and trace element core–rim profiles of garnet from the muscovite granite.

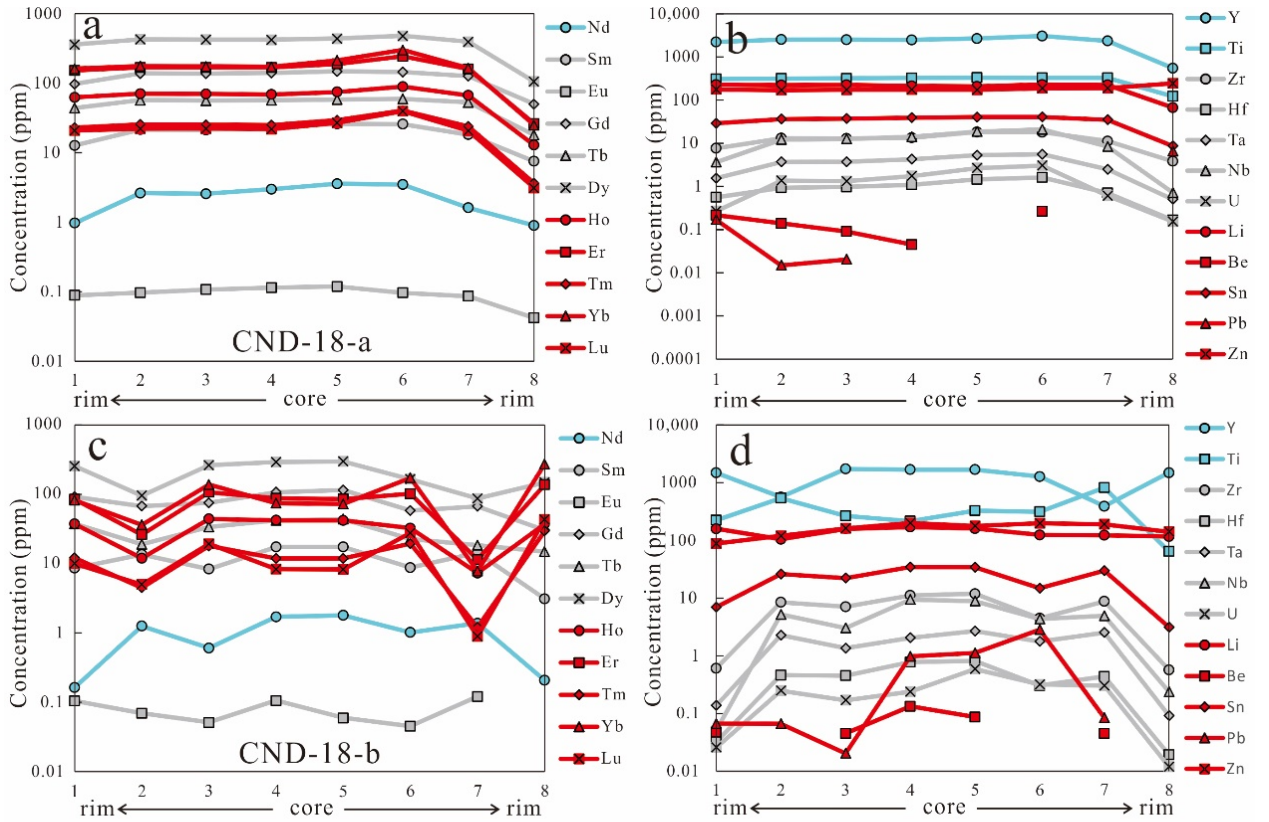

Figure 7. *Cont.*

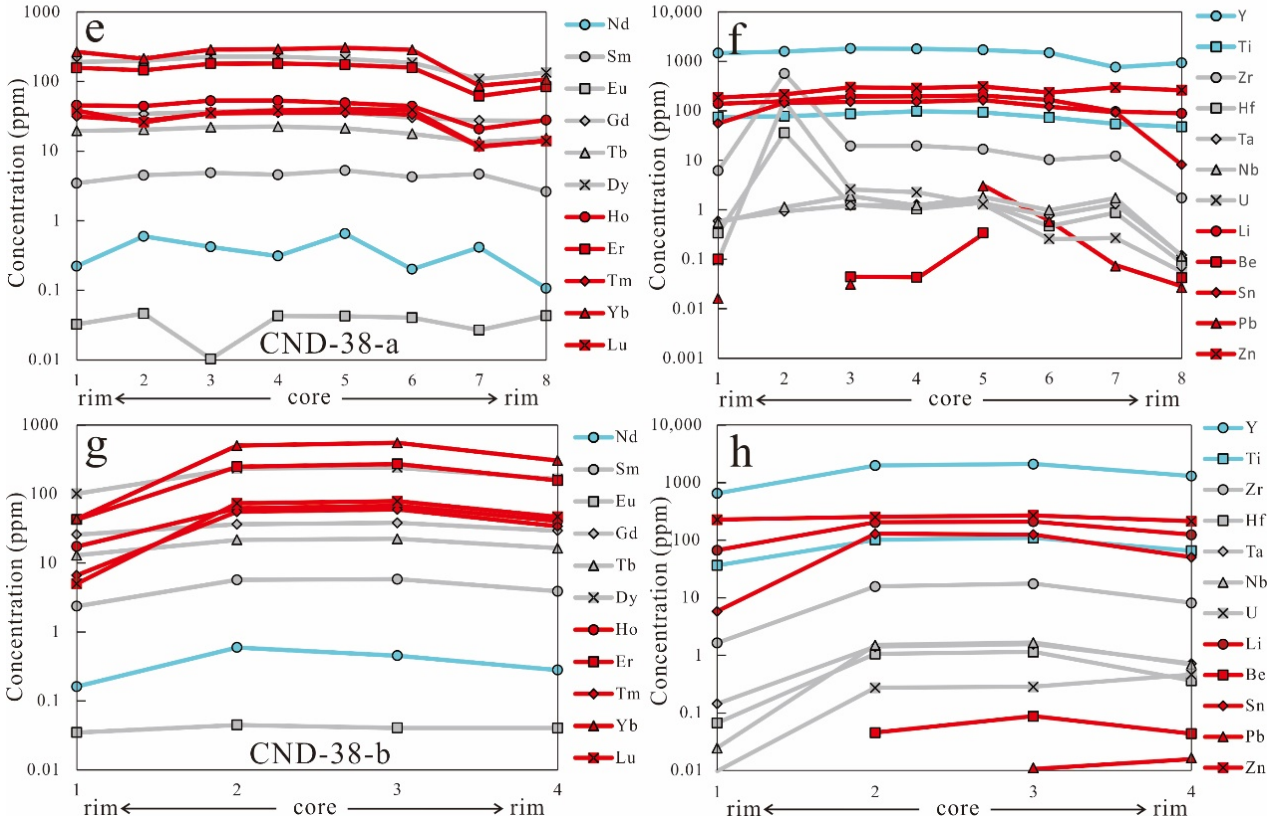

Figure 7. (**a**–**h**) Rare earth element and trace element core–rim profiles of garnet from the pegmatite.

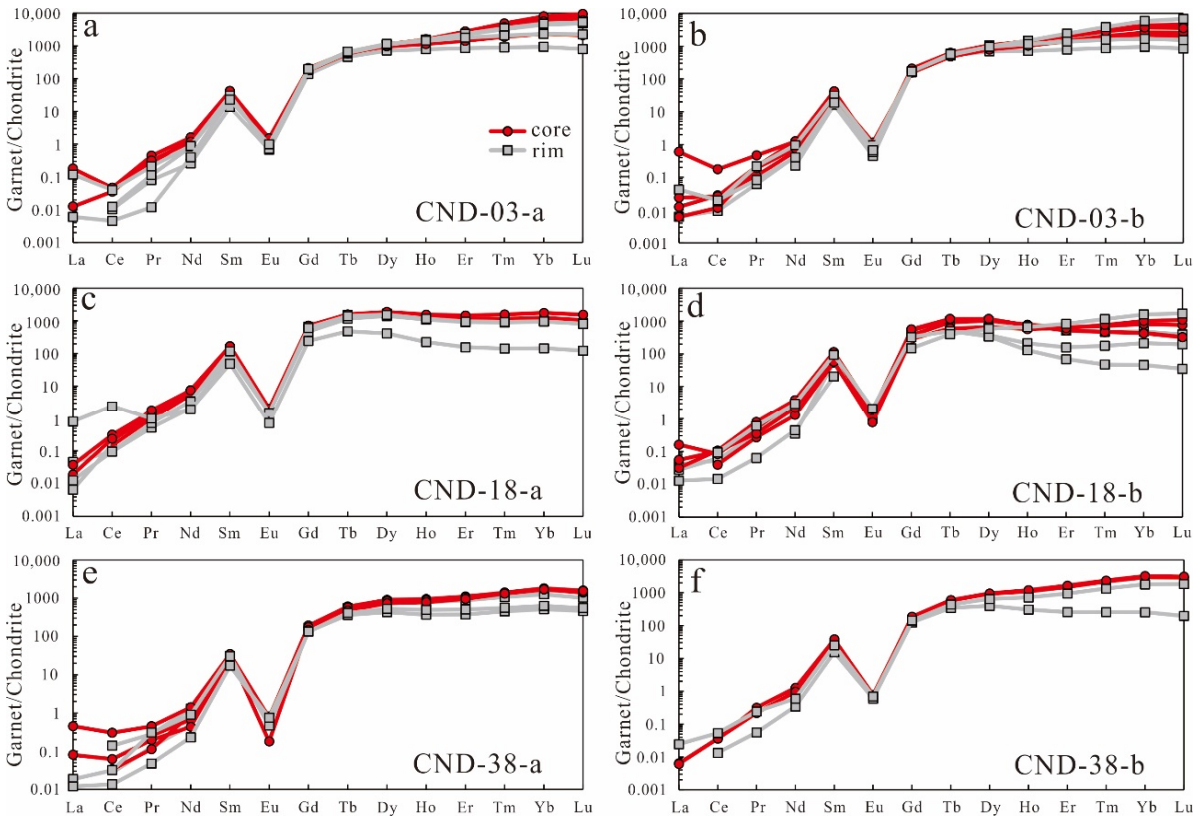

Figure 8. Chondrite-normalized REE patterns of garnets: (**a**,**b**) garnets from the muscovite granite; (**c**–**f**) garnets from the pegmatite (chondrite normalization data from [63]).

5.3. Zoning Textures

Overall, the garnets from the muscovite granite and pegmatite exhibit zoning with rim-ward spessartine depletion and almandine enrichment trends, except for sample CND–18, which shows a complex and/or irregular variation pattern (Figure 4). However, it is important to note that sample CND–18 shows grossular enrichment sharply towards the rim (Figure 4c,d). Element mapping suggests that the grain CND–03–a has higher Mn and lower Fe contents in the extremely narrow rim compared to the mantle (Figure 9). In addition, garnets from the pegmatite show enrichment of HREE and Y in the core (Figures 5c–f, 7, and 8c–f). In contrast, the HREE and Y zonings in garnets from the muscovite granite are inconspicuous (Figures 6 and 8a,b). The zonation in all the analyzed garnets is less prominent for MREE, Li, and Zn (Figures 6 and 7). Diagrams show that the rim-ward depletion trends of Zr, Hf, Nb, Ta, and U are similar to those of Nd and Sn (Figures 5–7).

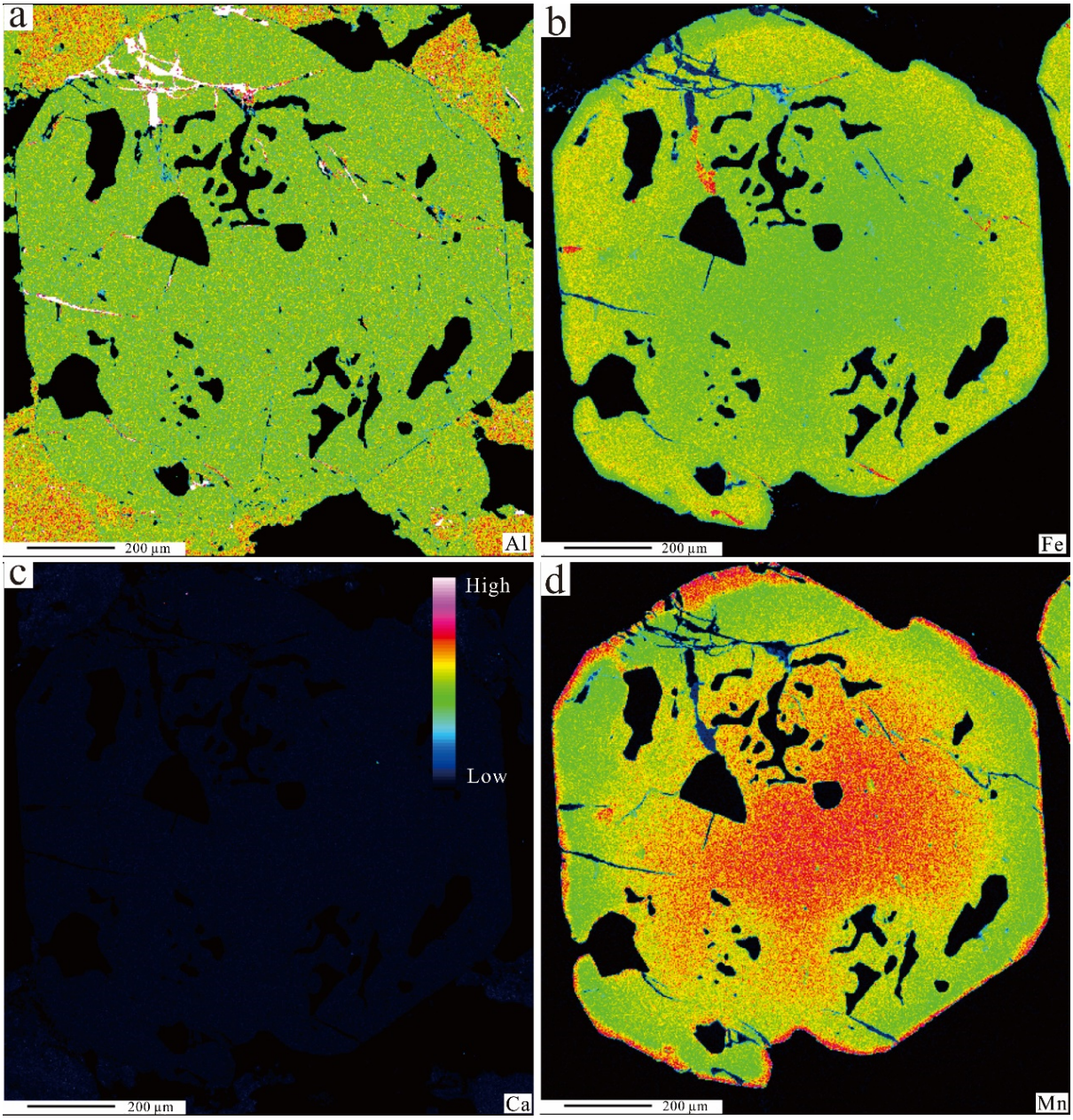

Figure 9. Element maps of Al (**a**), Fe (**b**), Ca (**c**), and Mn (**d**) for the garnet CND–03–a from the muscovite granite.

6. Discussion

6.1. Chemical Zoning in Garnet

The normal zoning, which is Mn-rich in the core and Fe-rich in the rim, is the dominant type, indicating primary growth [64]. Such a garnet is generally thought to be formed at conditions of low nucleation density, high growth rate, and low cation diffusion rate [65].

Crystal growth is usually controlled by various factors, including magma conditions and dynamic processes, while the compositional zoning or chemical gradient is commonly controlled by chemical diffusion [21,65,66]. The possibility is that the compositional zoning affected by diffusion can be tested using the diffusivity data for Mn, Fe, Mg, and Ca in garnet [67]. The garnet is assumed to be a spherical body of defined size, with neither defects nor cracks, in an infinite reservoir of relevant chemical components. The time (t) necessary for an element to diffuse through a distance (X) in a sphere of radius (r) can be determined applying the equation of [68], $t = X^2 \times t'/D$, where D is the diffusion coefficient (m^2/s), $t' = 0.4$ for a sphere (X = r), and $t' = 0.03$ for a hollow sphere (X < r). The diameter of the garnets in this study roughly varies between ~0.5×10^{-3} and ~1.5×10^{-3} m. By using the diffusivities of [67], the time for the Mn-enriched core to re-equilibrate with the rim compositions ranges from 8×10^6 to 7×10^7 yr. Previous studies suggested that the timescale of magmatic processes producing gr·anitic magmas, from melting to crystallization, rarely exceeds 10^5 years [22,69,70]. Therefore, it seems that chemical diffusion had little or no effect on the compositional zoning documented in the Cuonadong garnets.

6.2. Origin of Garnet

Garnets in granitic rocks have been studied by many scholars and their origin has been explained by various models: (1) the refractory restite phase [71]; (2) the peritectic entrainment phase from the zone of partial melting [22,72,73]; (3) xenocrysts sourced from assimilated country rocks [24,74,75]; (4) crystals formed at higher pressures ($P \geq 7$ kb) [70,76–79]; and (5) crystallization from strongly peraluminous melts at low pressure or from post-magmatic fluids or highly fractionated and Mn-enriched magma [80–83]. Firstly, neither garnet-bearing xenoliths in the leucogranites (muscovite granite and pegmatite) nor metamorphic mineral inclusions and reaction rims in the garnet were found. Furthermore, minerals in the leucogranites are typically igneous. Secondly, previous studies have shown that the leucogranites were derived from crustal melts [34,57,84,85] and garnets in this study were formed at low pressure (see Section 6.3). Thirdly, the garnets are euhedral to subhedral and equilibrate with other minerals, lacking resorption processes. Lastly, the garnets are predominately presented by an almandine–spessartine solid solution with a relatively high percentage of spessartine molecules and MnO content (Figure 4), which is consistent with garnets from pegmatites or highly fractionated granites [54,81]. In addition, all the analyzed garnets of the leucogranites fall in the range of magmatic compositions (Figures 10 and 11) and exhibit characteristics of HREE enrichment and significantly negative Eu anomalies (Figure 8), resembling that of garnet crystallizing from a highly evolved melt [21,29,70,86]. Therefore, the garnets in this study are typical magmatic garnets.

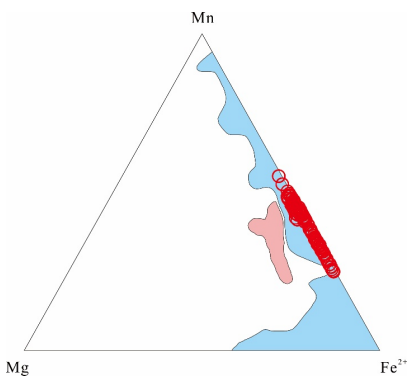

Figure 10. Mn–Mg–Fe ternary diagram. The pink area represents the magmatic garnet field from

S-type granite [21], and the light blue area represents the magmatic garnet field from [87]. Garnets from the muscovite granite and pegmatite fall in the field of magmatic garnet reported by [87].

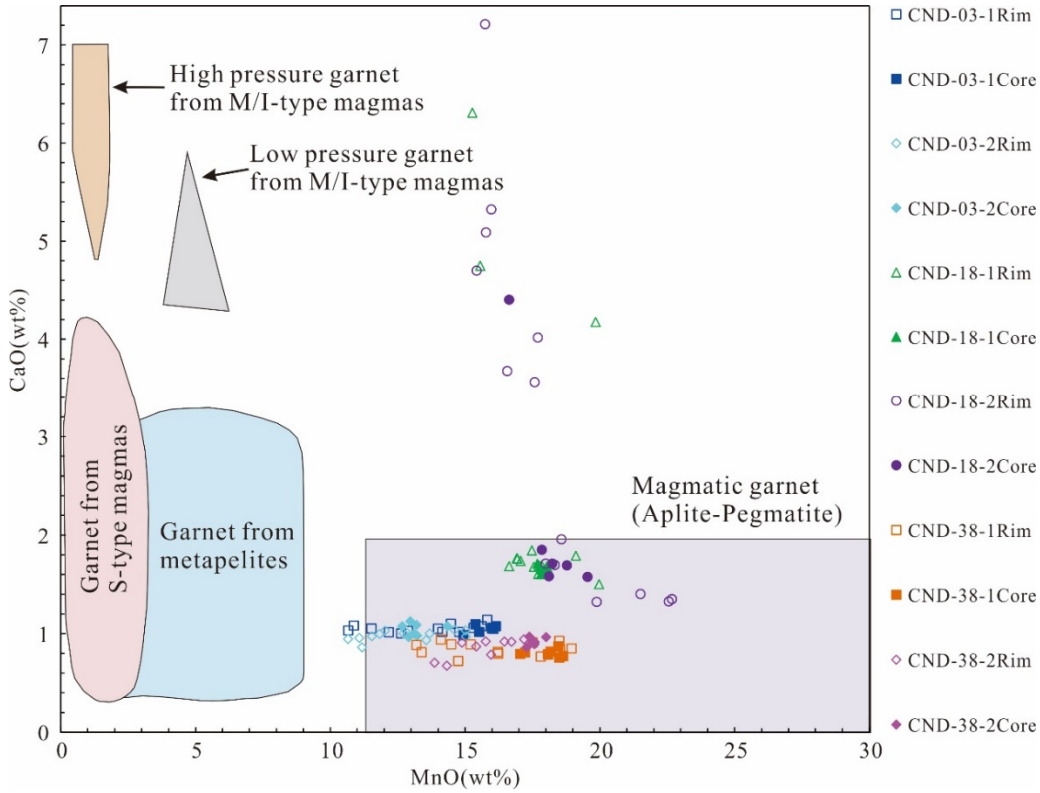

Figure 11. CaO versus MnO (wt%) diagram (modified after [70,77,81,82]). The compositions of garnets from the muscovite granite and pegmatite dominantly lie in the magmatic garnet field (aplite-pegmatite).

6.3. P-T Conditions of Garnet Crystallization

It has been generally accepted that magmatic garnets in granitic rocks formed at above ~700 °C display inverse bell-shaped profiles with respect to spessartine (rim-ward Mn enrichment) or are generally spessartine unzoned. However, garnet showing a bell-shaped profile concerning Mn may be magmatic and formed in highly evolved magmas (SiO_2 = 73–76wt%) crystallizing at low temperatures (<~700 °C) or are metamorphic (xenocrystic garnet) [21,88]. While garnets in sample CND–18 show fluctuating Mn profiles, the garnets in the muscovite granite and pegmatite are commonly characterized by bell-shaped spessartine profiles (Figure 4), indicating that garnet crystallization occurred below 700 °C. This is roughly consistent with the zircon saturation temperatures (662–711 °C, [31,57]) of the leucogranites from the Cuonadong region and other northern Himalayan leucogranites [11,31,34,57].

Previous studies have shown that Mn-rich garnets with 20–25 mol% spessartine may crystallize at shallow levels (below 5 kbar) and possibly to shallower depths (1–3 kbar) with higher Mn contents [21,69,89]. The garnets in the muscovite granite and pegmatite have high MnO (>10 wt%) and spessartine (>25 mol%) compositions, indicating a low-pressure condition. In general, the CaO contents are relatively low in garnets from the muscovite granite and pegmatite, although garnets in the sample CND–18 of pegmatite show rim-enriched grossular contents (Figure 4c,d and Figure 11). In addition, the occurrence of muscovite in the leucogranites indicates that the magma crystallizes at a maximum temperature of ~710 °C and a maximum pressure of 3.8 kbar [90]. Hence, in any case, although no accurate geothermobarometer is available, the geological, compositional, and textural features demonstrate that the garnets from the leucogranites formed at moderately low temperatures and relatively low-pressure conditions.

6.4. Implications for Evolution Process of Magma

The crystal texture and chemical composition of garnets usually record the evolution process of magma and magmatic–hydrothermal fluids and are important indicators to trace the compositions, properties, and environmental changes of fluids [18,20,81–83]. During the process of magma crystallization, generally represented by a Mn-rich almandine–spessartine solid solution or spessartine, the garnet is usually a mineral crystallized in the late stage of magma crystallization and fractionation. With an increasing degree of fractionation, the MnO and spessartine contents and/or MnO/(MnO + FeO) ratio of garnet gradually increase [64,81,91,92]. The MnO concentration, spessartine content, and MnO/(MnO + FeO) ratio of garnets from the Cuonadong dome all increase from the muscovite granite (10.7–16.1 wt%; 24.8–38.0 mol%; 0.243–0.375) to the pegmatite (13.2–22.7 wt%; 31.2–53.4 mol%; 0.305–0.545) (Table S1), indicating that the degree of magma fractionation increases from the muscovite granite to the pegmatite.

Garnet is enriched with trace elements such as REE, Hf, Zn, and Y, which can indicate the formation environment of the pegmatite magma and the evolution process of the granitic magma [18,20]. The aqueous medium-acidic silic-aluminous magma system usually goes through three stages from formation, migration, and cooling to finally complete solidification: (1) the magmatic stage—the system mainly exists in the melt phase and crystal phase; (2) the magmatic–hydrothermal transition stage—the system is characterized by the coexistence of a melt phase, crystal phase, and fluid phase; and (3) the hydrothermal stage—the system is dominated by a fluid phase and crystal phase, and the melt phase gradually disappears [93–95].

HREE and Y are compatible elements in garnets. When garnet is combined with minor or no HREE- and Y-bearing minerals (e.g., xenotime, thorite, and zircon), the contents of HREE and Y in garnet gradually increase with the enhancement of the evolution degree [18,96,97]. However, the contents of Y and HREE in garnets gradually decrease from the muscovite granite to the pegmatite with the evolution of magma (Figures 6–8), and garnets in the pegmatite display rim-ward HREE and Y depletion trends. Moreover, these HREE- and Y-bearing minerals are scarce in these pegmatites according to our observation. The distribution coefficients of Y and REE in garnet are negatively correlated with the content of fluid and the degree of magma evolution [28,98]. Thus, the lower HREE and Y contents in garnets from the pegmatite and the depletion of HREE and Y at the garnet rim in the pegmatite suggest a fluid-rich melt at the late stage of evolution. After the magmatic evolution to pegmatite, the system entered a fluid-rich environment, which led to the decrease of Y and HREE in garnet. Therefore, as the degree of magma evolution increased, the garnets from the pegmatite likely crystallized from a lower-temperature fluid. As a result, the contents of Y and HREE in garnet and/or the garnet rim in the pegmatite gradually decrease.

In addition, the garnets in sample CND–18 of the pegmatite show rim-ward enrichment of grossular and CaO contents (Figure 4c,d). This phenomenon is indicative of the interaction of magmatic fluids with previously crystallized minerals or country rocks and incorporation of Ca into a highly fractionated granitic body [83,99]. Thus, the increasing grossular and CaO contents of the garnet rim in the pegmatite may reflect an influence of fluids in their composition.

7. Conclusions

(1) The degree of fractionation from the muscovite granite to the pegmatite gradually increases in the Cuonadong dome. Garnets in the muscovite granite and in the pegmatite are dominated by an almandine–spessartine solid solution, and these garnets exhibit Mn, HREE, and Y zonings and are magmatic in origin.
(2) Garnets from the Cuonadong leucogranites formed at moderately low temperatures and relatively low-pressure conditions.
(3) Garnets from the Cuonadong leucogranites are characterized by HREE enrichment and LREE depletion, with significant Eu anomalies. From the muscovite granite to the

pegmatite, the contents of HREE and Y in garnets gradually decrease, which indicates the crystallization from a lower-temperature fluid of garnets from the pegmatite. Elevated grossular and CaO contents of the garnet rim from the pegmatite may reflect an influence of fluids in their composition.

(4) Garnet can be used as an indicator of magma evolution in these leucogranites.

Supplementary Materials: The following supporting information can be downloaded at: https://www.mdpi.com/article/10.3390/min12101275/s1, Table S1. Major element compositions (wt%) and structural formula of garnets from the muscovite granite and pegmatite; Table S2. Trace and rare earth element concentrations (ppm) of garnets from the muscovite granite and pegmatite. Notes: '-' represents the content below detection limit.

Author Contributions: Conceptualization, H.Y. and D.Y.; methodology, H.Y.; software, D.Y.; validation, H.Y.; formal analysis, D.Y.; investigation, C.M. and S.W.; resources, H.Y.; data curation, S.W. and C.M.; writing—original draft preparation, D.Y.; writing—review and editing, H.Y. and D.Y.; visualization, H.Y.; supervision, D.Y. All authors have read and agreed to the published version of the manuscript.

Funding: This research was funded by the Guangdong Major Project of Basic and Applied Basic Research, grant number (2019B030302013).

Data Availability Statement: Data sharing is not applicable to this article.

Conflicts of Interest: The authors declare no conflict of interest.

References

1. Hou, Z.Q.; Zheng, Y.C.; Zeng, L.S.; Gao, L.E.; Huang, K.X.; Li, W.; Li, Q.Y.; Fu, Q.; Liang, W.; Sun, Q.Z. Eocene-Oligocene granitoids in southern Tibet: Constraints on crustal anatexis and tectonic evolution of the Himalayan Orogen. *Earth Planet Sci. Lett.* **2012**, *349–350*, 38–52. [CrossRef]
2. Zheng, Y.C.; Hou, Z.Q.; Fu, Q.; Zhu, D.C.; Liang, W.; Xu, P.Y. Mantle inputs to Himalayan anatexis: Insights from petrogenesis of the Miocene Langkazi leucogranite and its dioritic enclaves. *Lithos* **2016**, *264*, 125–140. [CrossRef]
3. Wu, F.Y.; Liu, Z.C.; Liu, X.C.; Ji, W.Q. Himalayan leucogranite: Petrogenesis and implications to orogenesis and plateau uplift. *Acta Petrol. Sin.* **2015**, *31*, 1–36. (In Chinese with English Abstract).
4. Wu, F.Y.; Liu, X.C.; Liu, Z.C.; Wang, R.C.; Xie, L.; Wang, J.M.; Ji, W.Q.; Yang, L.; Liu, C.; Khanal, G.P.; et al. Highly fractionated Himalayan leucogranites and associated rare-metal mineralization. *Lithos* **2020**, *352–353*, 105319. [CrossRef]
5. Li, G.M.; Zhang, L.K.; Jiao, Y.J.; Xia, X.B.; Dong, S.L.; Fu, J.G.; Liang, W.; Zhang, Z.; Wu, J.Y.; Dong, L.; et al. First discovery and implications of Cuonadong superlarge Be-W-Sn polymetallic deposit in Himalayan metallogenic belt, southern Tibet. *Miner. Depos.* **2017**, *36*, 1003–1008. (In Chinese with English Abstract).
6. Wang, R.C.; Wu, F.Y.; Xie, L.; Liu, X.C.; Wang, J.M.; Yang, L.; Lai, W.; Liu, C. A preliminary study of rare-metal mineralization in the Himalayan leucogranite belts, South Tibet. *Sci. China Earth Sci.* **2017**, *60*, 1655–1663. [CrossRef]
7. Huang, C.M.; Li, G.M.; Zhang, Z.; Liang, W.; Huang, Y.; Zhang, L.K.; Fu, J.G. Petrogenesis of the Cuonadong leucogranite in South Tibet: Constraints from bulk-rock geochemistry and zircon U-Pb dating. *Earth Sci. Front.* **2018**, *25*, 182–195. (In Chinese with English Abstract).
8. Xie, L.; Tao, X.; Wang, R.; Wu, F.; Liu, C.; Liu, X.; Li, X.; Zhang, R. Highly fractionated leucogranites in the eastern Himalayan Cuonadong dome and related magmatic Be-Nb-Ta and hydrothermal Be-W-Sn mineralization. *Lithos* **2020**, *354-355*, 105286. [CrossRef]
9. Cao, H.W.; Li, G.M.; Zhang, R.Q.; Zhang, Y.H.; Zhang, L.K.; Dai, Z.W.; Zhang, Z.; Liang, W.; Dong, S.L.; Xia, X.B. Genesis of the Cuonadong tin polymetallic deposit in the Tethyan Himalaya: Evidence from geology, geochronology, fluid inclusions and multiple isotopes. *Gondwana Res.* **2021**, *92*, 72–101. [CrossRef]
10. Dai, Z.W.; Li, G.M.; Xie, Y.L.; Yang, Z.M.; Marten Huizenga, J.; Liang, W.; Fu, J.G.; Cao, H.W. Source and evolution of the ore-forming fluid of the Cuonadong Sn-W-Be polymetallic deposit (southern Tibet, China): Constraints from scheelite trace element and Sr isotope geochemistry. *Ore Geol. Rev.* **2022**, *142*, 104570. [CrossRef]
11. Zhang, D.C.; Zhang, G.Y.; Chen, X.; Yang, B. Mineralogical characteristics of highly fractionated leucogranite in Cuonadong dome, southern Tibet. *Acta Petrol. Mineral.* **2021**, *40*, 1093–1115. (In Chinese with English Abstract).
12. Orajaka, I.P. Geochemistry of Kaffo Valley albite–riebeckite–granite, Liruei Granite ring-complex, northern Nigeria. *Chem. Geol.* **1986**, *56*, 85–92. [CrossRef]
13. Ben, T.X.; Hoai, N.V.; Visnepskaya, Y.E. The behaviour of rare metals in Piaoac granite massif, Vietnam. *J. Southeast Asian Earth Sci.* **1993**, *8*, 383–386.
14. Huang, D.H.; Wu, C.Y.; Han, J.Z. Petrology, REE geochemistry and rock-forming mechanism of the Zudong and Guangxi granites, Jiangxi Province. *Bull. Chin. Acad. Geol. Sci.* **1993**, *27*, 69–94. (In Chinese with English Abstract).

15. Piccoli, P.; Candela, P.; Rivers, M. Interpreting magmatic processes from accessory phases: Titanite—a small-scale recorder of large-scale processes. *Trans. R. Soc. Edinb. Earth Sci.* **2000**, *91*, 257–267.
16. Wang, R.C.; Hu, H.; Zhang, A.C.; Xu, S.J.; Wang, D.Z. Yttrium zoning in garnet from the Xihuashan granitic complex and its petrological implications. *Chin. Sci. Bull.* **2003**, *48*, 1611–1615. (In Chinese with English Abstract). [CrossRef]
17. Li, X.H.; Li, W.X.; Wang, X.C.; Li, Q.L.; Liu, Y.; Tang, G.Q. Role of mantle-derived magma in genesis of early Yanshanian granites in the Nanling Range, South China: In situ zircon Hf-O isotopic constraints. *Sci. China Ser. D Earth Sci.* **2009**, *52*, 1261–1278. (In Chinese with English Abstract). [CrossRef]
18. Yang, J.H.; Peng, J.T.; Hu, R.Z.; Bi, X.W.; Zhao, J.H.; Fu, Y.Z.; Shen, N.P. Garnet geochemistry of tungsten-mineralized Xihuashan granites in South China. *Lithos* **2013**, *177*, 79–90. [CrossRef]
19. Dutrow, B.L.; Henry, D.J. Tourmaline compositions and textures: Reflections of the fluid phase. *J. Geosci.* **2018**, *63*, 99–110. [CrossRef]
20. Fu, J.G.; Li, G.M.; Dong, S.L.; Zhang, H.; Guo, W.K.; Zhang, L.K.; Liang, W.; Jiao, Y.J.; Ling, C. Mineral chemistry of garnet and its implication for the magmatic-hydrothermal transition in rare metal leucogranites in the Lalong dome, southern Tibet, China. *Sediment. Geol. Teth. Geol.* **2022**, *42*, 288–299. (In Chinese with English Abstract).
21. Dahlquist, J.A.; Galindo, C.; Pankhurst, R.J.; Rapela, C.W.; Alasino, P.H.; Saavedra, J.; Fanning, C.M. Magmatic evolution of the Peñón Rosado granite: Petrogenesis of garnet-bearing granitoids. *Lithos* **2007**, *95*, 177–207. [CrossRef]
22. Villaros, A.; Stevens, G.; Buick, I.S. Tracking S-type granite from source to emplacement: Clues from garnet in the Cape granite suite. *Lithos* **2009**, *112*, 217–235. [CrossRef]
23. Lackey, J.S.; Dramann, S.; Hark, J.S.; Nowak, R.M. Tracing garnet origins in granitoid rocks by oxygen isotope analysis: Examples from the South Mountain batholith, Nova Scotia. *Can. Mineral.* **2011**, *49*, 417–439. [CrossRef]
24. Scallion, K.L.; Jamieson, R.A.; Barr, S.M.; White, C.E.; Erdmann, S. Texture and composition of garnet as a guide to contamination of granitoid plutons: An example from the Governor Lake area, Meguma Terrane, Nova Scotia. *Can. Mineral.* **2011**, *49*, 441–458. [CrossRef]
25. Wang, R.C.; Fontan, F.; Chen, X.M.; Hu, H.; Liu, C.S.; Xu, S.J. Accessory minerals in the Xihuashan Y-enriched granitic complex, Southern China: A record of magmatic to hydrothermal stage of evolution. *Can. Mineral.* **2003**, *41*, 727–748. [CrossRef]
26. Breiter, K.; Čopjakova, R.; Škoda, R. The involvement of F, CO_2, and As in the alteration in the Hora Svaté Kateriny A-type granite, Czech Republic. *Can. Mineral.* **2009**, *47*, 1375–1398. [CrossRef]
27. Smith, M.P.; Henderson, P.; Jeffries, T.E.R.; Long, J.; Williams, C.T. The Rare Earth Elements and Uranium in Garnets from the Beinn an Dubhaich Aureole, Skye, Scotland, UK: Constraints on Processes in a Dynamic Hydrothermal System. *J. Petrol.* **2004**, *45*, 457–484. [CrossRef]
28. Gaspar, M.; Knaack, C.; Meinert, L.D.; Moretti, R. REE in skarn systems: A LA-ICP-MS study of garnets from the Crown Jewel gold deposit. *Geochim. Cosmochim. Acta* **2008**, *72*, 185–205. [CrossRef]
29. Gao, L.E.; Zeng, L.S.; Shi, W.G.; Chen, Z.Y.; Hu, M.Y.; Sun, D.Y. Two types of garnets in the Cenozoic granites from the Himalayan Orogenic Belt: Geochemical characteristics and implications for crustal anatexis. *Acta Petrol. Sin.* **2012**, *28*, 2963–2980. (In Chinese with English Abstract).
30. Baghban, S.; Hosseinzadeh, M.R.; Moayyed, M.; Mokhtari, M.A.A.; Gregory, D.D.; Nia, H.M. Chemical composition and evolution of the garnets in the Astamal Fe-LREE distal skarn deposit, Qara-Dagh–Sabalan metallogenic belt, Lesser Caucasus, NW Iran. *Ore Geol. Rev.* **2016**, *78*, 166–175. [CrossRef]
31. Xie, J.J. Geochronology and Geochemistry of the Cuonadong and Cuora Leucogranites in Cuona Area, South Tibet. Master's Thesis, University of Chinese Academy of Sciences, Beijing, China, 2018; pp. 1–97. (In Chinese with English Abstract).
32. Dai, Z.W.; Li, G.M.; Ding, J.; Zhang, L.K.; Cao, H.W.; Zhang, Z.; Liang, W. Chemical and boron isotopic composition, and significance of tourmaline from the Cuonadong tourmaline granite, Tibet. *Earth Sci.* **2019**, *44*, 1849–1859, (In Chinese with English Abstract).
33. Xia, X.B.; Li, G.M.; Cao, H.W.; Liang, W.; Fu, J.G. Petrogenic age and geochemical characteristics of the mother rock of skarn type ore body in the Cuonadong Be-W-Sn polymetallic deposit, southern Tibet. *Earth Sci.* **2019**, *44*, 2207–2223. (In Chinese with English Abstract).
34. Yang, B. Geochemical characteristics and diagenetic age of the leucogranites in the Cuonadong, Tibet. Master's Thesis, Chengdu University of Technology, Chengdu, China, 2019; pp. 1–70. (In Chinese with English Abstract).
35. Thiede, R.C.; Arrowsmith, J.R.; Bookhagen, B.; McWilliams, M.; Sobel, E.R.; Strecker, M.R. Dome formation and extension in the Tethyan Himalaya, Leo Pargil, northwest India. *Geol. Soc. Am. Bull.* **2006**, *118*, 635–650. [CrossRef]
36. Langille, J.; Lee, J.; Hacker, B.; Seward, G. Middle crustal ductile deformation patterns in southern Tibet: Insights from vorticity studies in Mabja Dome. *J. Struct. Geol.* **2010**, *32*, 70–85. [CrossRef]
37. Lee, J.; Hager, C.; Wallis, S.R.; Stockli, D.F.; Whitehouse, M.J.; Aoya, M.; Wang, Y. Middle to late Miocene extremely rapid exhumation and thermal reequilibration in the Kung Co rift, southern Tibet. *Tectonics* **2011**, *30*, 1–26. [CrossRef]
38. Liang, W.; Yang, Z.S.; Zheng, Y.C. The Zhaxikang Pb-Zn polymetallic deposit: Ar-Ar age of sericite and its metallogenic significance. *Acta Petrol. Sin.* **2015**, *89*, 560–568. (In Chinese with English Abstract).
39. Fu, J.G.; Li, G.M.; Wang, G.H.; Huang, Y.; Zhang, L.K.; Dong, S.L.; Liang, W. First field identification of the Cuonadong dome in southern Tibet: Implications for EW extension of the north Himalayan gneiss dome. *Int. J. Earth Sci.* **2017**, *106*, 1581–1596. [CrossRef]

40. Fu, J.G.; Li, G.M.; Wang, G.H.; Zhang, L.K.; Liang, W.; Zhang, X.Q.; Jiao, Y.J.; Dong, S.L. Syntectonic skarn characteristics and mineralization age of associated Be-W-Sn rare metal deposit in Cuonadong dome, southern Tibet, China. *J. Jilin Univ. (Earth Sci. Ed.)* **2020**, *50*, 1304–1322. (In Chinese with English Abstract).
41. Fu, J.G.; Li, G.M.; Wang, G.H.; Zhang, L.K.; Liang, W.; Zhang, X.Q.; Jiao, Y.J.; Huang, Y. Structural and thermochronologic constraints on skarn rare-metal mineralization in the Cenozoic Cuonadong Dome, Southern Tibet. *J. Asian Earth Sci.* **2021**, *205*, 104612. [CrossRef]
42. Yin, A.; Harrison, T. Geologic evolution of the Himalayan-Tibetan Orogen. *Annu. Rev. Earth Planet. Sci.* **2000**, *28*, 211–280. [CrossRef]
43. Zeng, L.S.; Gao, L.E.; Tang, S.H.; Hou, K.J.; Guo, C.L.; Hu, G.Y. Eocene magmatism in the Tethyan Himalaya, southern Tibet. *Geol. Soc.* **2014**, *412*, 287–316. [CrossRef]
44. Zhang, H.F.; Harris, N.; Parrish, R.; Zhang, L.; Zhao, Z.D.; Li, D.W. Geochemistry of north Himalayan Leucogranites: Regional comparison, petrogenesis and tectonic implications. *Earth Sci.-J. China Univ. Geosci.* **2005**, *30*, 275–288. (In Chinese with English Abstract).
45. Liu, Z.C.; Wu, F.Y.; Liu, X.C.; Wang, J.G.; Yin, R.; Qiu, Z.L.; Ji, W.Q.; Yang, L. Mineralogical evidence for fractionation processes in the Himalayan leucogranites of the Ramba Dome, southern Tibet. *Lithos* **2019**, *340-341*, 71–86. [CrossRef]
46. Le Fort, P. Himalayas: The collided range. Present knowledge of the continental arc. *Am. J. Sci.* **1975**, *275*, 1–44.
47. Harrison, T.M.; Lovera, O.M.; Grove, M. New insights into the origin of two contrasting Himalayan granite belts. *Geology* **1997**, *25*, 899–902. [CrossRef]
48. Hou, Z.Q.; Qu, X.M.; Yang, Z.S.; Meng, X.J.; Li, Z.Q.; Yang, Z.M.; Zheng, M.P.; Zheng, Y.Y.; Nie, F.J.; Gao, Y.F.; et al. Metallogenesis in Tibetan collisional orogenic belt: III. Mineralization in post-collisional extension setting. *Miner. Depos.* **2006**, *25*, 629–651. (In Chinese with English Abstract).
49. Qi, X.X.; Li, T.F.; Meng, X.J.; Yu, C.L. Cenozoic tectonic evolution of the Tethyan Himalayan foreland fault-fold belt in southern Tibet, and its constraint on antimony-gold polymetallic minerogenesis. *Acta Petrol. Sin.* **2008**, *24*, 1638–1648. (In Chinese with English Abstract).
50. Nie, F.J.; Hu, P.; Jiang, S.H.; Li, Z.Q.; Liu, Y.; Zhou, Y.Z. Type and temporal-spatial distribution of gold and antimony deposits (prospects) in southern Tibet, China. *Acta Geol. Sin.* **2005**, *79*, 373–385. (In Chinese with English Abstract).
51. Yang, Z.S.; Hou, Z.Q.; Meng, X.J.; Liu, Y.C.; Fei, H.C.; Tian, S.H.; Li, Z.Q.; Gao, W. Post-collisional Sb and Au mineralization related to the South Tibetan detachment system, Himalayan orogen. *Ore Geol. Rev.* **2009**, *36*, 194–212. [CrossRef]
52. Guillot, S.; Mah'eo, G.; de Sigoyer, J.; Hattori, K.H.; P^echer, A. Tethyan and Indian subduction viewed from the Himalayan high- to ultrahigh-pressure metamorphic rocks. *Tectonophysics* **2008**, *451*, 225–241. [CrossRef]
53. Fu, J.G.; Li, G.M.; Wang, G.H.; Zhang, L.K.; Liang, W.; Zhang, X.Q.; Jiao, Y.J.; Dong, S.L.; Huang, Y. Structural analysis of sheath folds and geochronology in the Cuonadong dome, southern Tibet, China: New constraints on the timing of the South Tibetan detachment system and its relationship to North Himalayan gneiss domes. *Terra Nova* **2020**, *32*, 300–323. [CrossRef]
54. Zhang, Z.; Zhang, L.K.; Li, G.M.; Liang, W.; Xia, X.B.; Fu, J.G.; Dong, S.L.; Ma, G.T. The Cuonadong gneiss dome of North Himalaya: A new member of gneiss dome and a new proposition for the ore-controlling role of North Himalaya gneiss domes. *Acta Geosci. Sin.* **2017**, *38*, 754–766. (In Chinese with English Abstract).
55. He, C.T.; Qin, K.Z.; Li, J.X.; Zhou, Q.F.; Zhao, J.X.; Li, G.M. Preliminary study on occurrence status of beryllium and genetic mechanism in Cuonadong tungsten-tin-beryllium deposit, eastern Himalaya. *Acta Petrol. Sin.* **2020**, *36*, 3593–3606. (In Chinese with English Abstract).
56. Liang, W.; Li, G.M.; Basang, Y.D.; Zhang, L.K.; Fu, J.G.; Huang, Y.; Zhang, Z.; Wang, Y.Y.; Cao, H.W. Metallogenesis of Himalaya gneiss dome: An example from Cuonadong gneiss dome in Zhaxikang ore concentration area. *Miner. Depos.* **2021**, *40*, 932–948. (In Chinese with English Abstract).
57. Lin, B.; Tang, J.X.; Zheng, W.B.; Leng, Q.F.; Lin, X.; Wang, Y.Y.; Meng, Z.; Tang, P.; Ding, S.; Xu, Y.F.; et al. Geochemical characteristics, age and genesis of Cuonadong leucogranite, Tibet. *Acta Petrol. Mineral.* **2016**, *35*, 391–406.
58. Zhang, L.K.; Zhang, Z.; Li, G.M.; Dong, S.L.; Xia, X.B.; Liang, W.; Fu, J.G.; Cao, H.W. Rock assemblage, structural characteristics and genesis, mechanism of the Cuonadong dome, Tethys Himalaya. *Earth Sci.* **2018**, *43*, 2664–2683. (In Chinese with English Abstract).
59. Zhang, Z.; Li, G.M.; Zhang, L.K.; Dong, S.L.; Liang, W.; Fu, J.G.; Huang, Y.; Cao, H.W.; Xia, X.B. The early Oligocene beryl-bearing pegmatite in the Cuonadong dome, southern Tibet: Its forming mechanism and geological significances. *Sediment. Geol. Teth. Geol.* **2020**, *40*, 14–30. (In Chinese with English Abstract).
60. Dong, H.W.; Xu, Z.Q.; Meng, Y.K.; Yi, Z.Y. Geochronology of leucogranites in the Cuonadong dome, southern Tibet and limitation of the timing of the Southern Tibet Detachment System (STDS). *Acta Petrol. Sin.* **2017**, *33*, 3741–3752. (In Chinese with English Abstract).
61. Fu, J.G.; Li, G.M.; Wang, G.H.; Zhang, L.K.; Liang, W.; Zhang, Z.; Dong, S.L.; Huang, Y. Timing of E-W extension deformation in north Himalaya: Evidences from Ar-Ar age in the Cuonadong dome, south Tibet. *Earth Sci.* **2018**, *43*, 2638–2650. (In Chinese with English Abstract).
62. Liu, Y.S.; Gao, S.; Hu, Z.C.; Gao, C.G.; Zong, K.Q.; Wang, D.B. Continental and oceanic crust recycling-induced melt-peridotite interactions in the Trans-North China Orogen: U-Pb dating, Hf isotopes and trace elements in zircons from mantle xenoliths. *J. Petrol.* **2010**, *51*, 537–571. [CrossRef]

63. Sun, S.S.; Mcdonough, W.F. Chemical and isotopic systematics of oceanic basalts: Implications for mantle composition and processes. *Geol. Soc. Lond. Spec. Publ.* **1989**, *42*, 313–345. [CrossRef]
64. Bekele, B.; Kumar Sen, A. The mineral chemistry of gahnite, garnet and columbite-group minerals (CGM): Implications for genesis and evolution of the Kenticha Rare-element granite-pegmatite, Adola, Ethiopia. *J. Afr. Earth Sci.* **2020**, *162*, 103691. [CrossRef]
65. Manning, D.A.C. Chemical variation in garnets from aplites and pegmatites, peninsular Thailand. *Mineral. Mag.* **1983**, *47*, 353–358. [CrossRef]
66. Chakraborty, S.; Ganguly, J. Cation diffusion in aluminosilicate garnets: Experimental determination in spessartine-almandine diffusion couples, evaluation of effective binary diffusion coefficients, and applications. *Contrib. Mineral. Petrol.* **1992**, *111*, 74–86. [CrossRef]
67. Carlson, W.D. Rates of Fe, Mg, Mn, and Ca diffusion in garnet. *Am. Mineral.* **2006**, *91*, 1–11. [CrossRef]
68. Crank, J. *The Mathematics of Diffusion*; Oxford University Press: Oxford, UK, 1975; 414p.
69. Clemens, J.D.; Wall, V.J. Origin and crystallization of some peraluminous (S-type) granitic magmas. *Can. Mineral.* **1981**, *10*, 111–131.
70. Samadi, R.; Mirnejad, H.; Kawabata, H.; Harris, C.; Valizadeh, M.V.; Gazel, E. Magmatic garnet in the Triassic (215 Ma) Dehnow pluton of NE Iran and its petrogenetic significance. *Int. Geol. Rev.* **2014**, *56*, 596–621. [CrossRef]
71. René, M.; Stelling, J. Garnet-bearing granite from the Třebíč pluton, Bohemian massif (Czech Republic). *Mineral. Petrol.* **2007**, *91*, 55–69. [CrossRef]
72. Stevens, G.; Villaros, A.; Moyen, J.F. Selective peritectic garnet entrainment as the origin of geochemical diversity in S-type granites. *Geology* **2007**, *35*, 9–12. [CrossRef]
73. Jung, S.; Pfänder, J.A.; Mezger, K.; Hellebrand, E.; Brandt, S. Polyphase growth history of peritectic garnet from a granite: Trace-element zonation, Lu-Hf ages and their significance for the duration of granite-forming processes. *Lithos* **2022**, *418–419*, 106675. [CrossRef]
74. Allan, B.D.; Clarke, D.B. Occurrence and origin of garnets in the South Mountain Batholith, Nova Scotia. *Can. Mineral.* **1981**, *19*, 19–24.
75. Lackey, J.S.; Romero, G.A.; Bouvier, A.S.; Valley, J.W. Dynamic growth of garnet in granitic magmas. *Geology* **2012**, *40*, 171–174. [CrossRef]
76. Green, T.H. Experimental phase equilibrium studies of garnet-bearing I-type volcanics and high-level intrusives from Northland, New Zealand. Geological Society of America Special Papers. *Geol. Soc. Am.* **1992**, *272*, 429–438.
77. Harangi, S.Z.; Downes, H.; Kósa, L.; Szabo, C.S.; Thirlwall, M.F.; Mason, P.R.D.; Mattey, D. Almandine garnet in calc-alkaline volcanic rocks of the Northern Pannonian Basin (Eastern-Central Europe): Geochemistry, petrogenesis and geodynamic implications. *J. Petrol.* **2001**, *42*, 1813–1843. [CrossRef]
78. Patranabis-Deb, S.; Schieber, J.; Basu, A. Almandine garnet phenocrysts in a ~1 Ga rhyolitic tuff from central India. *Geol. Mag.* **2008**, *146*, 133–143. [CrossRef]
79. Narduzzi, F.; Farina, F.; Stevens, G.; Lana, C.; Nalini, H.A., Jr. Magmatic garnet in the Cordilleran-type Galiléia granitoids of the Araçuaí belt (Brazil): Evidence for crystallization in the lower crust. *Lithos* **2017**, *282-283*, 82–97. [CrossRef]
80. Whitworth, M.P. Petrogenetic implications of garnets associated with lithium pegmatites from SE Ireland. *Mineral. Mag.* **1992**, *56*, 75–83. [CrossRef]
81. Rahmani Javanmard, S.; Tahmasbi, Z.; Ding, X.; Khalaji-Ahmadi, A.; Hetherington, C.J. Geochemistry of garnet in pegmatites from the Boroujerd Intrusive Complex, Sanandaj-Sirjan Zone, western Iran: Implications for the origin of pegmatite melts. *Mineral. Petrol.* **2018**, *112*, 837–856. [CrossRef]
82. Qin, Q.; Wang, T.; Huang, H.; Zhang, Z.C.; Tong, Y.; Song, P.; Zhang, J.J. Late Carboniferous and Early Permian garnet-bearing granites in the South Tianshan Belt, NW China: Two Late Paleozoic magmatic events and implications for crustal reworking. *J. Asian Earth Sci.* **2021**, *220*, 104923. [CrossRef]
83. Quelhas, P.; Mata, J.; Alveirinho-Dias, A. Magmatic Evolution of Garnet-Bearing highly Fractionated Granitic Rocks from Macao, Southeast China: Implications for Granite-Related Mineralization Processes. *J. Earth Sci.* **2021**, *32*, 1454–1471. [CrossRef]
84. Liu, X.C.; Li, X.H.; Liu, Y.; Yang, L.; Li, Q.L.; Wu, F.Y.; Yu, H.M.; Huang, F. Insights into the origin of purely sediment-derived Himalayan leucogranites: Si-O isotopic constraints. *Sci. Bull.* **2018**, *63*, 1243–1245. [CrossRef]
85. Hopkinson, T.N.; Harris, N.B.W.; Warren, C.J.; Spencer, C.J.; Roberts, N.M.W.; Horstwood, M.S.A.; Parrish, R.R.; EIMF. The identification and significance of pure sediment-derived granites. *Earth Planet. Sci. Lett.* **2017**, *467*, 57–63. [CrossRef]
86. Taylor, R.J.M.; Harley, S.L.; Hinton, R.W.; Elphick, S.; Clark, C.; Kelly, N.M. Experimental determination of REE partition coefficients between zircon, garnet and melt: A key to understanding high-Tcrustal processes. *J. Metamorph. Geol.* **2015**, *33*, 231–248. [CrossRef]
87. Miller, C.F.; Stoddard, E.F. The role of manganese in the paragenesis of magmatic garnet: An example from the Old Woman Piute Range, California. *J. Geol.* **1981**, *89*, 233–246. [CrossRef]
88. Nakano, T.; Ishikawa, Y. Chemical zoning of pegmatite areas, garnets northeastern from the Ishikawa Japan and Yamanoo. *Geochem. J.* **1997**, *31*, 105–118. [CrossRef]
89. Weisbrod, A. Étude experimentale de l'équilibre grenat-cordiérite dans le système Mn-Fe-Al-Si-O-H, à 750 °C. Implications thermodynamiques et pétrologiques. *Bulletin de la Société Française Minéralogie et de Cristallographie* **1974**, *97*, 261–270. [CrossRef]

90. Kerrick, D.M. Experimental determination of muscovite+quartz stabiliy with $p_{H_2O} < p_{total}$. *Am. J. Sci.* **1972**, *272*, 946–958. [CrossRef]
91. Černý, P. Exploration Strategy and Methods for Pegmatite Deposits of Tantalum. In *Lanthanides, Tantalum and Niobium*; Springer: New York, NY, USA, 1989; pp. 274–302.
92. Müller, A.; Kaersley, A.; Spratt, J.; Seltmann, R. Petrogenetic implications of magmatic garnet in granitic pegmatites from southern Norway. *Can. Mineral.* **2012**, *50*, 1095–1115. [CrossRef]
93. Zhu, J.C.; Wu, C.N.; Liu, C.S.; Li, F.C.; Huang, X.L.; Zhou, D.S. Magmatic-hydrothermal evolution and genesis of Koktokay No.3 rare metal pegmatite dyke, Altai, China. *Geol. J. China Uni.* **2000**, *6*, 40–52. (In Chinese with English Abstract).
94. Badanina, E.V.; Veksler, I.V.; Thomas, R.; Syritso, L.F.; Trumbull, R.B. Magmatic evolution of Li-F, rare-metal granites: A case study of melt inclusions in the Khangilay complex, Eastern Transbaikalia (Russia). *Chem. Geol.* **2004**, *210*, 113–133. [CrossRef]
95. Kaeter, D.; Barros, R.; Menuge, J.F.; Chew, D.M. The magmatic-hydrothermal transition in rare-element pegmatites from southeast Ireland: LA-ICP-MS chemical mapping of muscovite and columbite-tantalite. *Geochim. Cosmochim. Acta* **2018**, *240*, 98–130. [CrossRef]
96. Pyle, J.M.; Spear, F.S. Yttrium zoning in garnet: Coupling of major and accessory phases during metamorphic reactions. *Geol. Mater. Res.* **1999**, *1*, 1–49.
97. Feng, Y.G.; Lei, R.X.; Ju, M.H.; Song, G.S.; Xu, F. Origin and petrogenetic implications of garnet from Rb-rich pegmatites in North Qinling Orogen, China. *Geol. J.* **2017**, *52*, 215–237. [CrossRef]
98. Green, T.H.; Blundy, J.D.; Adam, J. SIMS determination of trace element partition coefficients between garnet, clinopyroxene and hydrous basaltic liquids at 2–7.5 GPa and 1080–1200 °C. *Lithos* **2000**, *53*, 165–187. [CrossRef]
99. Martin, R.F.; De Vito, C. The late-stage miniflood of Ca in granitic pegmatites: An open-system acid-reflux model involving plagioclase in the exocontact. *Can. Mineral.* **2014**, *52*, 165–181. [CrossRef]